Available online at www.CivileJournal.org

Civil Engineering Journal

(E-ISSN: 2476-3055; ISSN: 2676-6957)

Vol. 11, No. 02, February, 2025

Numerical Analysis of the Shear Behavior of Shallow-Wide Concrete Beams via the Concrete Damage Plasticity Model

Hewan Dejene [1, 2*], Muluken Bogale [2], Marina Rynkovskaya [1]

[1] Department of Construction Technology and Structural Materials, RUDN University, Moscow 117198, Russia.

[2] Faculty of Civil Engineering, Arba Minch Institute of Technology, Arba Minch University, Arba Minch 4400, Ethiopia.

Received 01 November 2024; Revised 19 January 2025; Accepted 25 January 2025; Published 01 February 2025

Abstract

Shallow reinforced concrete beams are broadly used in buildings for their aesthetic and economic benefits, but their shear performance remains insufficiently known, especially considering the impact of stirrups. While experimental investigations provide a good understanding, they are expensive and provide limited insight, creating a gap in the understanding of the complex shear behavior of shallow RC beams. This study bridges this limitation by conducting finite element analysis and calibrating the critical concrete damage plasticity parameters such as the dilation angle, Kc values, eccentricity, damage parameters, and loading time. Additionally, the numerical model validated the experimental results by accounting for the effects of the stirrup spacing, width, and longitudinal-to-stirrup ratio to achieve the ultimate load and corresponding deflection differences within 1.69% and 10.7%, respectively. The findings revealed that increasing the stirrup spacing enhanced ductility without increasing strength, whereas increasing the beam width and longitudinal-to-stirrup ratio increased strength and ductility. Finally, a comparison with design codes and machine learning revealed greater accuracy of FEA prediction, presenting new insight into upgrading the design code for shallow RC beams.

Keywords: Shallow RC Beams; Shear Behavior; Concrete Damage Plasticity Model; Finite Element Model; Abaqus.

1. Introduction

Recently, modern buildings have required efficient space utilization for architectural purposes, including higher and obstacle-free floor heights. Providing shallow reinforced concrete (RC) beams that are wider than twice as deep as the depth offers architectural flexibility, simple and quick formwork, and reduced cost [1-3]. Despite their decent resistance to shear stress, these beams are prone to shear failure after initiating a flexural crack [4, 5] or torsional crack [6], which prevents full flexural capacity development. Understanding and preventing this susceptibility is crucial for guaranteeing good structural performance. Experimental studies have investigated the factors that influence the shear strength of shallow RC beams. For example, Mahmoud et al. [6] studied the torsional behavior of seven wide beams, and reported that the load eccentricity, stirrup spacing, compressive strength, and longitudinal reinforcement ratio significantly affect the torsional capacity. Soliman et al. [2, 7] conducted multiple studies investigating the shear performance of fourteen shallow RC beams, revealing the significance of the concrete strength, width-to-depth ratio, shear reinforcement ratio, and arrangement. Elansary et al. [1] also proposed using spiral transverse reinforcement to improve ductility, although a slight strength improvement was achieved. Said et al. [8] experimentally explored how reducing the web reinforcement spacing improves the shear strength and ductility. While these studies provide critical insights, experimental approaches are expensive and limit detailed insight into structural behavior under loading.

* Corresponding author: hewandejene23@gmail.com; 1042235256@pfur.ru

http://dx.doi.org/10.28991/CEJ-2025-011-02-022

Finite element analysis (FEA) offers a cost-effective, time-efficient, and accurate alternative for studying the behavior of structural members. The key part of FEA is accurately modeling nonlinear material behavior such as cracking and crushing concrete, softening, aggregate interlocking, and rebars dowel action. Several material models, such as the Drucker–Prager theory, Continuum Damage Mechanics (CDM), and Concrete Damage Plasticity (CDP), have been presented to account for this nonlinearity [9-11]. The Drucker-Prager model is suitable for predicting the ultimate strength and postpeak behavior, the CDM model is appropriate for simulating material failure, and the CDP model combines both previous models to capture damage, plastic deformation, load–deflection response, and postpeak behavior. On the other hand, concrete behaves complexly and nonlinearly during loading, damaging high tensile and compressive stress zones, and the CDP model in the Abaqus module can adequately define this nonlinearity [12].

However, the accuracy of the CDP-based model relies primarily on the calibration and sensitivity analysis of the material parameters, mesh, and loading conditions. Various studies have explored the calibration of CDP parameters for structural members to identify critical parameters and optimal values for simulating structural elements. Behnam et al. [13] conducted a comprehensive sensitivity analysis for RC beam–column joints under cyclic loading and reported that a dilation angle of 40°, a Kc value of 0.667, and full damage parameters are critical for validating the experimental results. Raza et al. [14] studied rectangular RC columns reinforced with glass fiber polymer (GFRP) under axial loading and reported that a mesh size of 20 mm, viscosity of 0.0058, Kc value of 0.667, and dilation angle of 35° were critical parameters and were in good agreement with the experimental result.

Furthermore, Genikomsou et al. [15] also calibrated material parameters for RC slabs under cyclic loading; they reported that a dilation angle of 40°, damage parameters, and a mesh size of 20 mm were critical for accurately predicting the experimental result. Silva et al. [16] explored RC shear walls under axial loading and reported a dilation angle of 46.4°, a Kc value of 0.58, and a viscosity of 0.00001 for the optimized load–deflection response. Szczecina & Winnicki [17] also conducted a sensitivity analysis on the effects of loading time and viscosity on the modeling of RC structures. This finding emphasized the importance of calibrating and conducting a sensitivity analysis of CDP parameters for particular structural members, and loading is necessary. However, its implementation for shallow RC beams, specifically shear behavior, is still undiscovered. Design codes and studies, including ACI, Eurocode, FIB modal Code III, truss model, and genetic programming, offer empirical equations for predicting the shear strength of RC beams [18-22]. However, these design codes and studies are mainly used for conventional RC beams. They may not accurately predict or estimate the complex behavior of shallow RC beams, specifically by accounting for the effects of transverse reinforcement. Therefore, these design code predictions should be assessed and compared with comprehensive finite element models to ensure efficient and accurate design.

This study fills these gaps by conducting a comprehensive sensitivity analysis on critical CDP parameters of the shear performance of shallow RC beams via the FEA software Abaqus. The numerical model was subsequently used to validate the experimental results [2, 7] to assess the load–deflection curve, failure mechanisms, and crack patterns in detail. Following validation, the effects of the transverse reinforcement spacing, width-to-depth ratio, and the longitudinal-to-transverse reinforcement ratio on the shear behavior of these beams are investigated. Moreover, the FEA predictions are compared with design codes and study predictions from the ACI, Eurocode, Fib Modal Code III, truss model, and genetic programming to evaluate their applicability to shallow RC beams and their capacity to account for the effects of stirrups. The workflow of the study is presented in Figure 1.

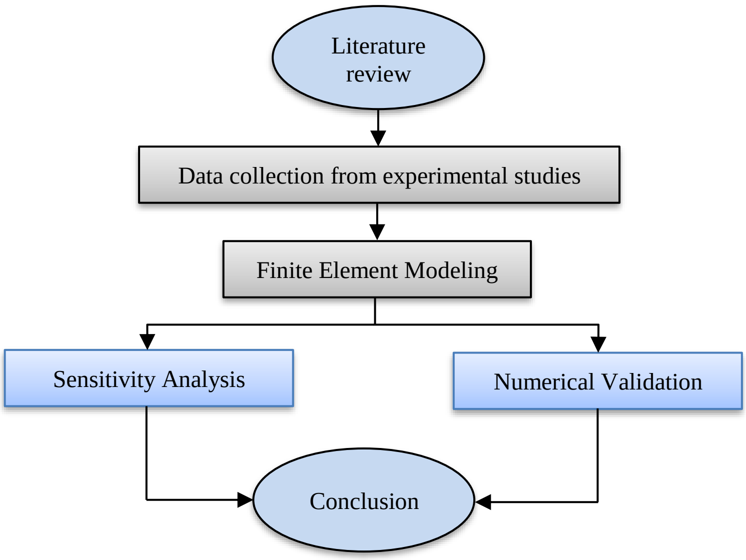

Figure 1. Workflow of the study

2. Description of the Experimental Investigation

Soliman et al. [7] studied the impact of transverse reinforcement on the shear behavior of seven shallow reinforced concrete beams under a three-point load, as shown in Figure 2. Two beams (B1 and B3) were selected to validate the numerical model. Both samples are 1200 mm long and 200 mm thick, with a compressive strength of 31 MPa. B1 has 8-mm-diameter four-leg stirrups with a width of 600 mm, twelve tension rebars (18 mm diameter), and eight compression rebars (10 mm diameter), as shown in Figure 3. B3, on the other hand, has 8-mm-diameter six-leg stirrups with a width of 900 mm, eighteen tension rebars (18 mm in diameter), and twelve compression rebars (10 mm in diameter), as shown in Figure 4. The yield strength for the longitudinal rebar is 416 MPa, and for the stirrups, it is 233 MPa.

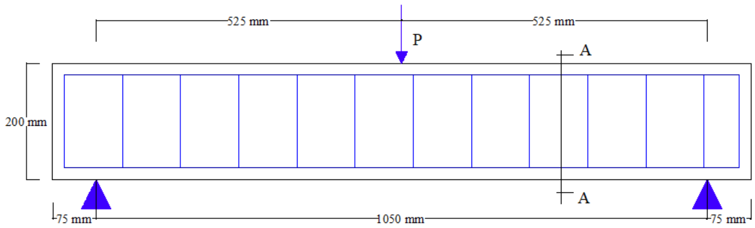

Figure 2. Layout of the shallow concrete beam

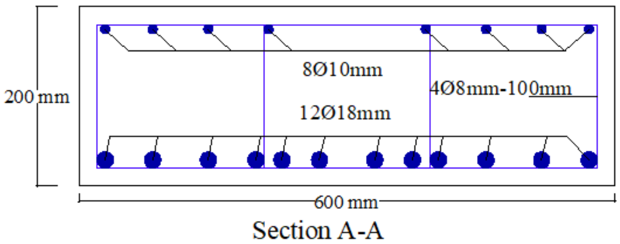

Figure 3. Beam detailing of B1

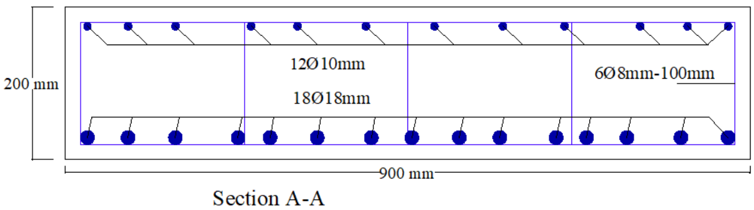

Figure 4. Beam detailing of B3

Soliman et al. [2] extended the experimental investigation to examine how the amount and arrangement of shear reinforcement affect seven shallow RC beams. In the present study, beam B2 was selected for numerical validation among seven beams. Figure 5 shows that B2 has the same characteristics as B1 and uses six-mm-diameter four-leg stirrups with 45 mm longitudinal spacing.

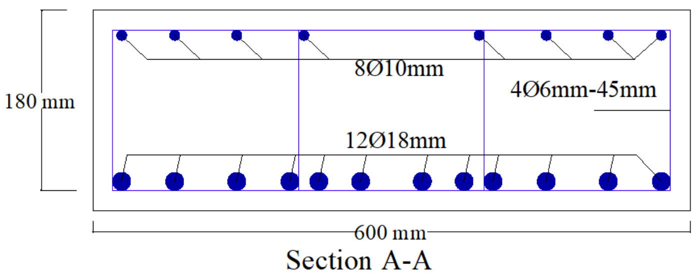

Figure 5. Beam detailing of B2

Tables 1 and 2 summarize the material properties of the reinforcement and concrete used in the experimental investigation.

Table 1. Reinforcement properties

Bar diameter	Beam type	Yield stress (MPa)	Ultimate stress (MPa)	Elastic modulus (MPa)	Poisson's ratio
6	B2	233	370	200,000	0.3
8	B1, B3	233	370	200,000	0.3
10	B1, B2, & B3	416	600	200,000	0.3
18	B1, B2, & B3	416	600	200,000	0.3

Table 2. Concrete properties

Beam type	Concrete strength (MPa)	Elastic Modulus (MPa)	Tensile strength (MPa)	Poisson's ratio
B1, B2 & B3	31	30.891	3.341	0.2

3. Finite Element (FE) Model

3.1. Element Type and Loading Conditions

A 3-D linear brick element with reduced integration (C3D8R) was used to model the concrete part from the Abaqus/standard module [23]. The longitudinal rebar and stirrups were simulated by a 2-node linear in space (B31). An embedded constraint was used in the interaction between the concrete and reinforcement, which prevents the translation of the reinforcement at the node. An analytically rigid element with high rigidity and stiffness was defined for the load pin and support to prevent deformation.

A reference point is attached to the bottom and upper surface of the support and load pin to define the boundary condition, as shown in Figures 6 to 8. A tie constraint is then defined at the contact surface of the beam and support pin to ensure compatibility throughout the loading process. A tie constraint is also used between the beam and the load pin. The constraints of the pin (U_x=U_y=U_z=0) and roller (U_x=U_y=0) are applied at the reference points of the support pin's right-hand and left-hand bottom sides, respectively. Displacement is used at the boundary condition of the load pin reference point to simulate the experimental loading.

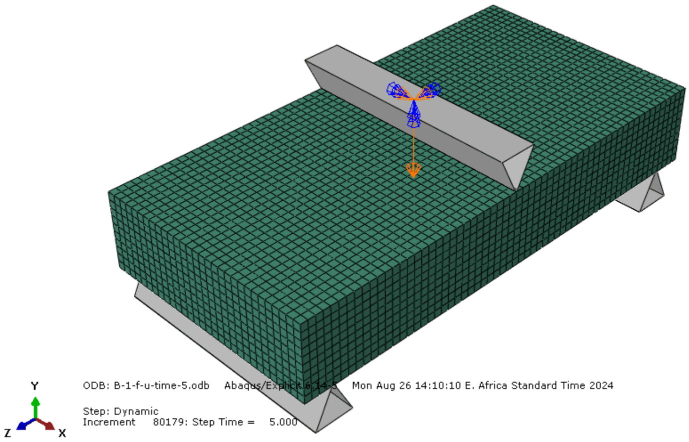

Figure 6. Model of the shallow beam

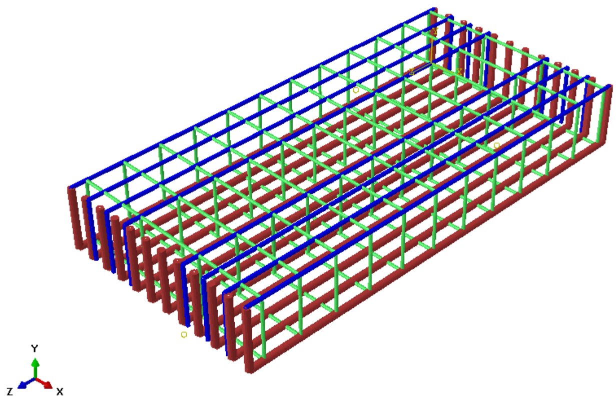

Figure 7. Model of the reinforcement

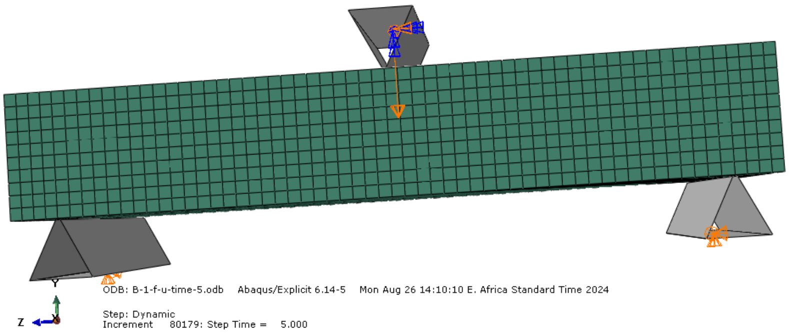

Figure 8. Boundary conditions and loading

3.2. Material Modeling

3.2.1. Concrete Modeling

Abaqus uses the concrete damage plasticity model to simulate the nonlinear properties of concrete by defining four parameters: plasticity, compressive behavior, tensile behavior, and damage parameters.

Concrete Plasticity

Plasticity defines the permanent deformation of concrete after the stress reaches the yield point, and the Drucker–Prager yield criterion describes this phenomenon. This plasticity behavior was captured by assigning five parameters: the dilation angle on the stress plane (ψ), the eccentricity of the flow (e), the ratio between the biaxial and uniaxial compressive yield stresses (fbo/fbc), the yield surface on the tensile meridian to the compressive meridian (k_c), and the relaxation time or viscosity (μ). Table 3 shows the default CDP parameter values used for the model.

Table 3. The CDP parameter used for the model

Test	ψ	e	fbo/fbc	K_c	μ
Soliman et al. [2, 7]	30	0.1	1.16	0.67	0.01

Compressive Strength of the Concrete

Eurocode [19] provides a three-phase stress–strain model to express the behavior of concrete under compressive stress, as illustrated in Figure 9. In the initial stage, concrete demonstrates an elastic linear stress-strain relationship up to stress values of $\sigma_c=0.4f_{cm}$, expressed in Equation 1. The stress–strain relationship subsequently becomes nonlinear, and the stress reaches its ultimate value of $\sigma c=fcm$. In the final stage, the stress–strain properties of the concrete begin to soften, as expressed in Equation 3.

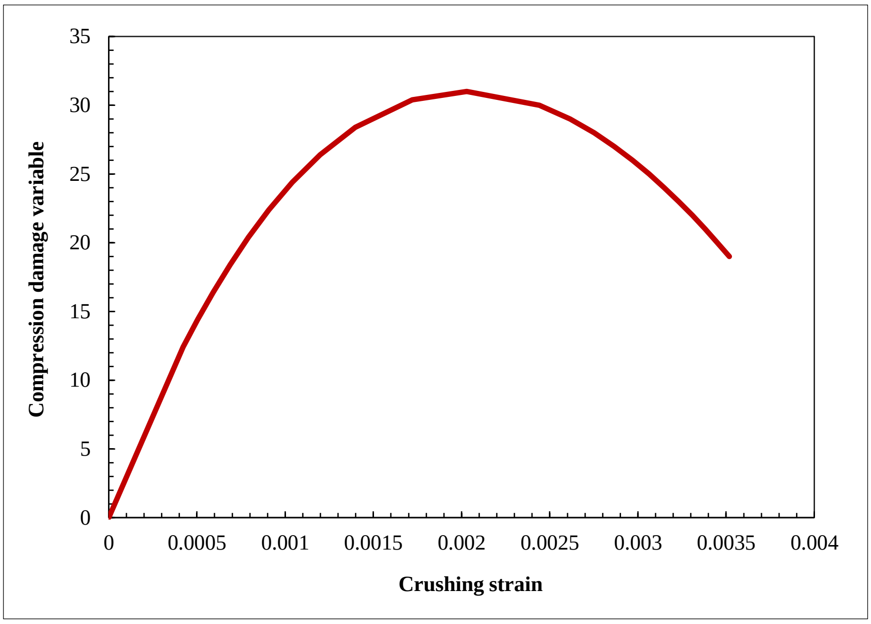

Figure 9. Uniaxial stress–strain diagram for compressive strength

$$\sigma c = Ecm * \mathcal{E}c;\ 0 \leq \mathcal{E}c \leq \left(\frac{0.4fcm}{Ecm}\right) \tag{1}$$

$$Ecm = 22 * (fcm)^{0.3} \tag{2}$$

$$\frac{\sigma c}{fcm} = \frac{k*\left(\frac{\varepsilon c}{\varepsilon 1}\right) - \left(\frac{\varepsilon c}{\varepsilon 1}\right)^2}{1+(k-2)*\left(\frac{\varepsilon c}{\varepsilon 1}\right)};\ \left(\frac{0.4*fcm}{Ecm}\right) \leq \mathcal{E}c \leq \mathcal{E}cu = 0.0035 \tag{3}$$

$$k = \frac{1.05*Ecm*|\varepsilon 1|}{fcm} \tag{4}$$

where $\varepsilon c1$ represents the strain at the ultimate strength, *fcm* represents the ultimate strength of the concrete, and εcu represents the failure strain. *Ecm* and $\mathcal{E}c$ represent the initial elastic modulus and strain, respectively.

Tensile Strength of the Concrete

Allam et al. [24] proposed a tension–stiffening stress–strain response for concrete under uniaxial tensile stress, as shown in Figure 10. The tensile stress on the concrete initially exhibits a linear elastic property until it reaches failure stress at the values of f_{ctm}, which can be calculated via Equation 5. After that, microcracks form on the concrete surface, leading to softening of the stress–strain response and the formation of significant cracks.

$$f_{ctm} = 0.3 * fcm^{\frac{2}{3}} \tag{5}$$

where f_{ctm} is the ultimate tensile stress, and where $\mathcal{E}cr$ is the strain at the ultimate stress.

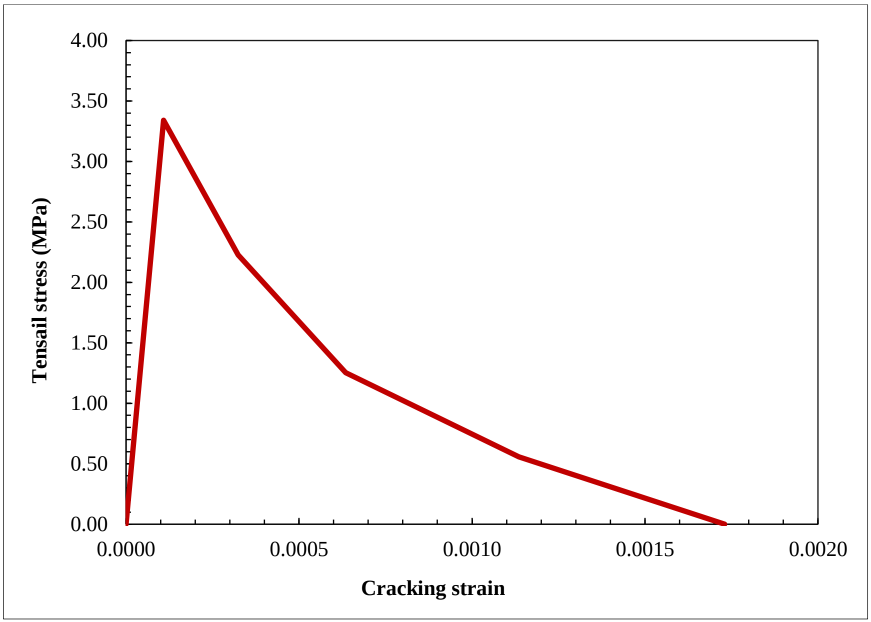

Figure 10. Uniaxial stress–strain diagram for tensile strength

Damage Evolution of Concrete

In the elastic stage, concrete unloading does not impact the elastic modulus; however, in the softening stage, the elastic modulus decreases. This failure initiation and stiffness degradation can be defined via the compressive (*dc*) and tensile damage variables (*dt*), as shown in Figures 11 and 12. The following equation can expresses this damage evolution:

$$dc = 1 - \ \sigma c/\sigma c, max \tag{6}$$

$$dt = 1 - \ \sigma t/\sigma t, max \tag{7}$$

where σc and σt are arbitrary compressive and tensile stresses and where $\sigma c,\ max,$ and $\sigma t,\ max$ are the ultimate compressive and tensile stresses, respectively.

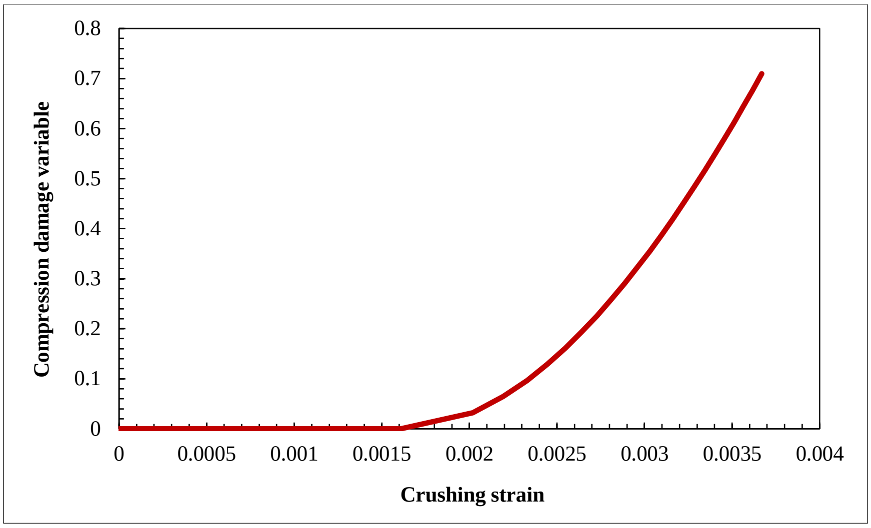

Figure 11. Compression damage parameter

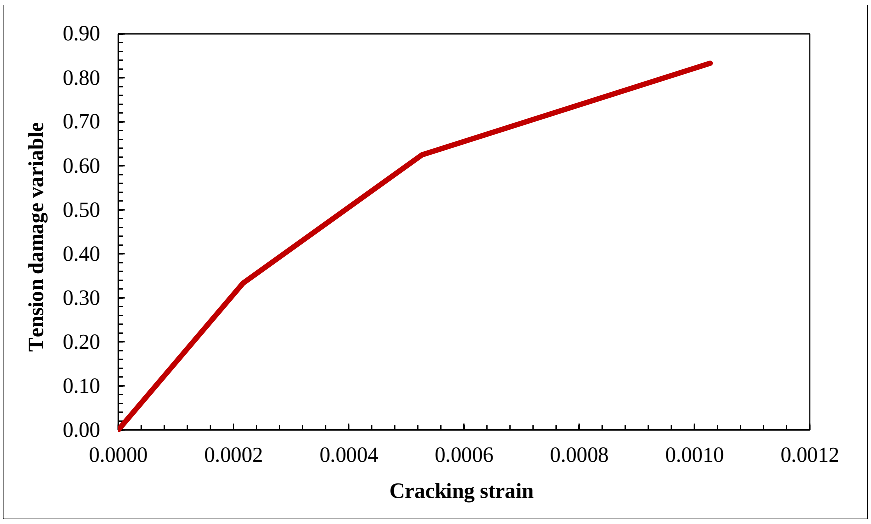

Figure 12. Tensile damage parameter

3.2.2. Reinforcement material properties

A bilinear stress–strain response is used to simulate the nonlinear characteristics of the reinforcement, as shown in Figure 13. The stress–strain response exhibits elastic linear behavior before the yield strain; beyond that, the strain hardens with a slope of 0.01.

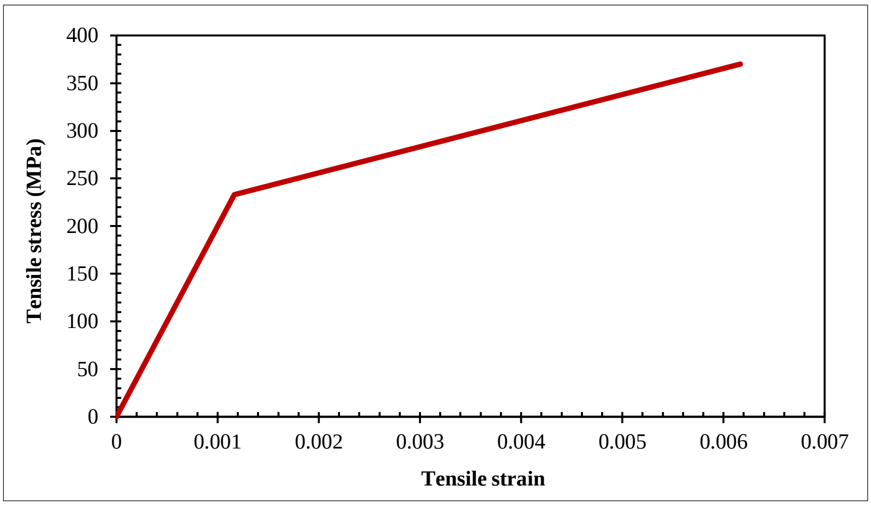

Figure 13. Stress–strain diagram of the reinforcement

4. Investigation of Material Parameters

Before calibration, beam B2 was chosen as a control beam to study the sensitive parameter in the concrete damage plasticity model. The calibration process accounts for the effects of CDP parameters such as the dilation angle, eccentricity, K_c values, damage parameters, loading time, and mesh size. Once the CDP parameters were calibrated, they were applied to the FE model of the remaining three wide beams.

The FEA software Abaqus offers two options for static analysis: standard (static) analysis with viscosity regularization or explicit (quasi-static) analysis using a longer loading time. Moreover, static analysis depends heavily on the viscosity parameter and requires more computational time; quasi-static analysis is significantly influenced by the loading time. Additionally, Szczecina & Winnicki [17] suggested that using lower viscosity values with higher loading times results in an optimal solution for quasi-static analysis. This study investigated the effect of loading time on the load–displacement response of control Samples with a constant viscosity of 0 for various loading times (0.5, 1, 5, and 10 s). The loading time significantly influenced the load–deflection response of the RC shallow beam, as shown in Figure 14.

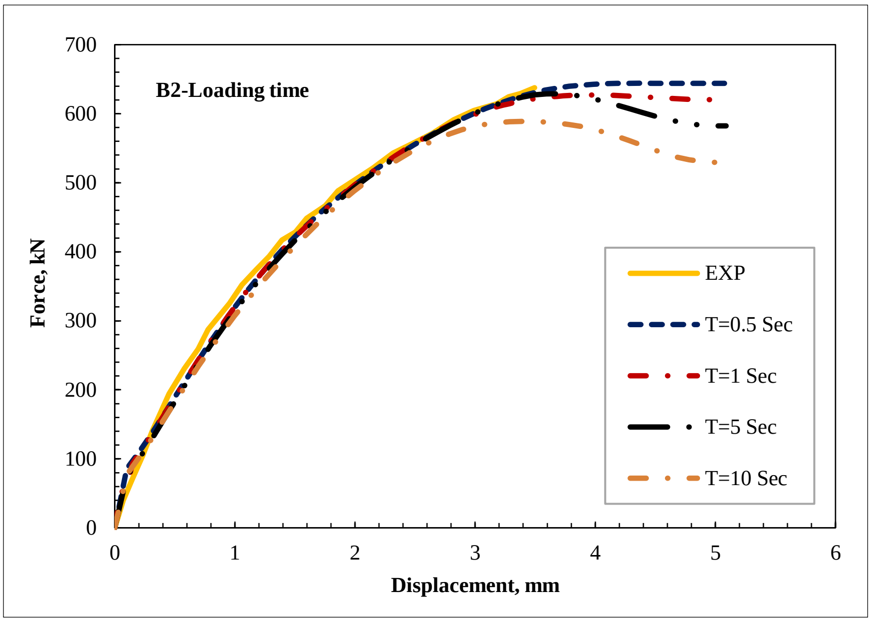

Figure 14. Influence of loading time

The load–deflection curve exhibited a stiffer response and higher ultimate load for a shorter loading time (0.5-1 second). This behavior occurs because concrete shows rate-dependent stiffness at lower loading times, reducing micro-crack development (overestimating tensile strength) and the occurrence of inertial effects. However, as the loading time increased from 0.5 to 1 second, the computational time nearly doubled, as shown in Table 4. Additionally, the kinetic to internal energy (KE/IE) ratio for a 0.5-second loading time was 0.08, far exceeding the recommended minimum inertial effect (0.002) for quasi-static analysis. This suggests that inertial effects significantly influence the analysis and diverge from the assumed quasi-static analysis.

Table 4. Summary of loading time, computational time, and kinetic-to-internal energy ratio

Loading time (Second)	Computational time (minute)	KE/IE
0.5	5	0.08
1	11	0.0024
5	61	0.00049
10	92	0.00043

Conversely, the load–deflection curve shows more realistic behavior for longer loading (5-10 s). The gradual application of load allows the internal stresses and strain of concrete to be redistributed efficiently, resulting in a reduced ultimate load but stable analysis results. At a 5-second loading time, the ratio of KE/IE decreased significantly, indicating that inertial effects were minimized with enhanced load–deflection predictions. However, further increasing the loading time to 10 s produced slight KE/IE ratio reductions while sustaining greater computational time and moderate load–deflection prediction. On the bases of these findings, a loading time of 5 s and a viscosity of 0 were selected for modeling the remaining beams.

Concrete resists stress elastically up to the yield stress; however, it expands in volume after the yield limit, and a dilation angle characterizes this behavior. The plastic potential function captures this characteristic of concrete plasticity, which controls the direction of plastic strain increase during nonlinear concrete behavior, such as cracking and crushing [25]. The following equation mathematically expresses this function:

$$\breve{\varepsilon}^{p} = \lambda \frac{\partial G}{\partial f} \tag{8}$$

where $\breve{\varepsilon}^{p}$ is the plastic strain increment, λ is the plastic multiplier, G is the plastic potential function used in the CDP model, and f is the stress tensor. The following equations express these nonassociated Drucker–Prager hyperbolic functions of G:

$$G = \sqrt{(\varepsilon f_t \tan\psi)^2 + \bar{q}^2} - \bar{p}\tan\psi \tag{9}$$

where Ɛ is the eccentricity of the flow potential surface on the $\bar{p} - \bar{q}$ plane with values of 0.1, f_t expresses the tensile strength, ψ is the dilation angle, $\bar{p}$ is the hydrostatic pressure and $\bar{q}$ is the deviatoric stress.

On the basis of the literature, initial dilation angle values for different structural members are recommended. For Example, Genikomsou et al. [15] calibrated dilation angles within the ranges of 20° – 42° and identified 40° as optimal for RC slab–column joints. Behnam et al. [13] explored values between 31^0 and 42°, concluding that 40° provided accurate RC-wide beam–column connections. Similarly, Raza et al. [14] investigated a range of 30° – 45° and recommended 35° as preferable for GFRP RC columns. Silva et al. [16] examined the dilation angle in broader ranges from 30° to 50° and recommended 46.4° as the optimal value for shear walls.

On the bases of previous studies, an initial range of dilation angles from 30° – 46° was selected for calibration to ensure that model accurately predicted the volume expansion of the concrete under loading. Sensitivity analysis was subsequently conducted by iteratively analyzing the load–deflection behavior by varying the dilation angle, as shown in Figure 15. The sensitivity analysis revealed three key aspects: failure load, postpeak behavior, and stiffness. As the dilation angle increases, the shallow beam has a higher failure load on the load–deflection curves. The reason is that increasing the dilation angle results in high volume expansion and internal friction of the concrete under loading, resulting in stress redistribution and improved shear capacity. For dilation angles between 30^0 and 34^0, the postpeak behavior shows a flattened curve, which is consistent with the experimental investigation, indicating balanced ductile and stiff behavior in the softening stage. In contrast, dilation angles greater than 40^0 resulted in stiffer postpeak behavior, resulting in improved capacity with limited ductility. This finding recommends adapting the dilation angle between 30^0 and 34^0, which is suitable for ductile members, whereas a dilation angle greater than 40^0 is good for structural members that need greater strength and stiffness. On the basis of this sensitivity analysis, assigning a dilation angle of 32^0 is most suitable for calibrating the remaining samples and balancing the experimental observations' stiffness, strength, and softening behavior.

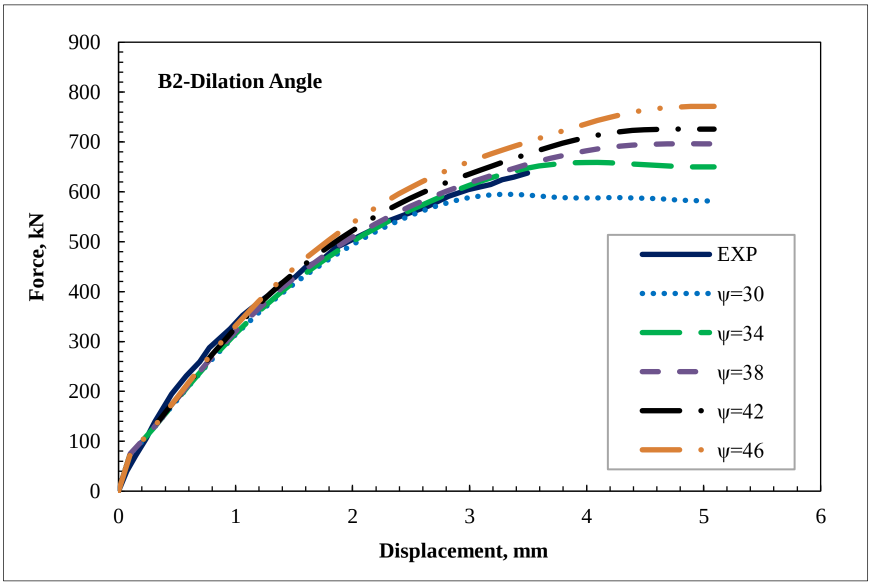

Figure 15. Influence of the dilation angle

The effect of the non-uniform distribution of stress on the yield surface was calibrated for different eccentricity values (0.1, 0.13, 0.16, and 0.2), as shown in Figure 16. The effects of eccentricity on the load and deflection were negligible. Therefore, the default eccentricity value of 0.1 was used for the rest of the modelling.

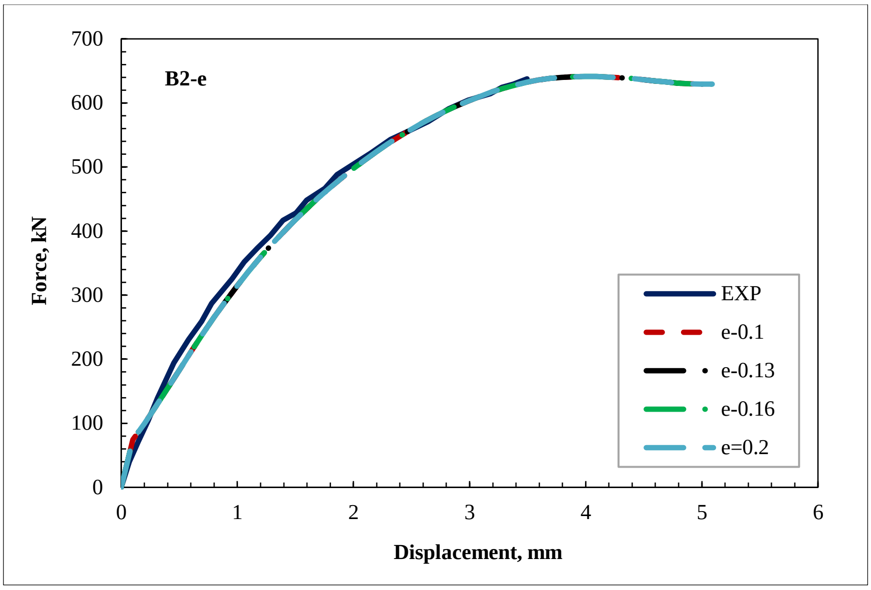

Figure 16. Influence of eccentricity

The parameter K_c represents the shape of the yield surface on the tensile and compressive meridians, which expresses the strength of the concrete against tensile and compressive stresses. The values of K_c range from 0.5 to 1, where 0.5 indicates high compressive strength with low tensile strength with an elliptical yield surface, and 1 expresses balanced strength under both tensile and compressive stresses of concrete with a circular yield surface. The initial K_c values (0.5, 0.667, 0.834, and 1) were chosen on the bases of prior research conducted by Wosatko et al. [25] and used as a basis for conducting sensitivity analysis to investigate the effects of K_c on the stiffness, ultimate load, and postpeak behavior through load–deflection analysis, as shown in Figure 17. The results showed that when K_c is 0.5, the numerical results yield a higher ultimate load than the experimental results do. This overestimation occurs because the elliptical yield surface assumes that the compressive strength resists more load than the tensile strength does, which delays the onset of yielding and failure. As K_c increases to 0.667, the numerical ultimate load prediction is improved. This improvement can be attributed to increasing K_c, reducing the compressive strength contribution, and providing a more balanced concrete behavior. In contrast, for K_c values of 0.834 and 1, the numerical results underestimate the ultimate load of the experimental result. This underestimation arises because the CDP model assumes equal resistance to tensile and compressive stresses, which misjudges the compressive strength.

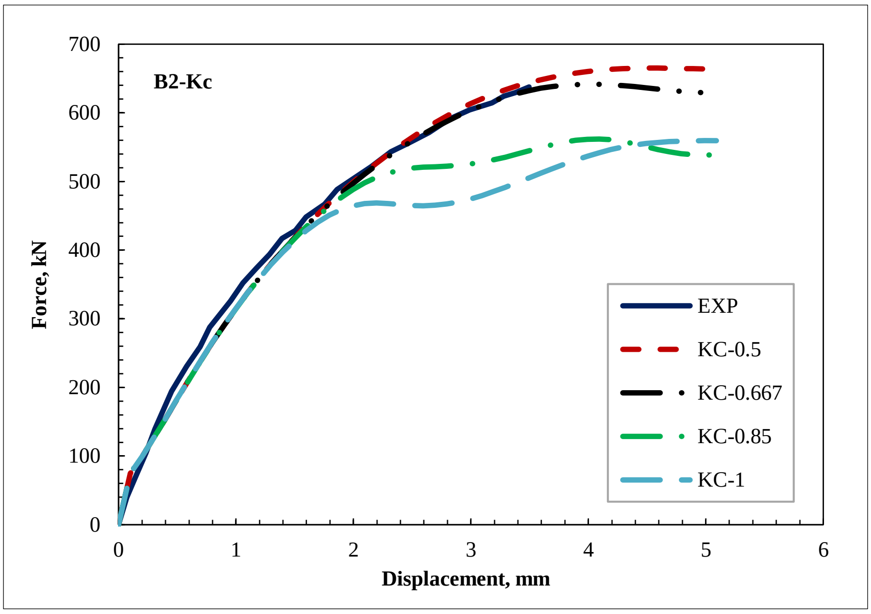

Figure 17. Influence of Kc values

The postpeak behavior further shows the influence of K_c. For K_c values of 0.5 and 0.667, the numerical result displays a steep softening curve, indicating a sudden loss of strength after the ultimate load. Conversely, for K_c values of 0.834 and 1, the analysis results in gradual softening, indicating flattened degradation of the load. However, all the

K_c values have similar initial stiffnesses, which align with the experimental results. Therefore, adjusting K_c near 0.5 best aligns with the behavior of the control samples in terms of load–deflection behavior and stiffness. Consequently, the kc value is adjusted to 0.667 for the remaining models.

The mesh sensitivity of the samples was evaluated with four different mesh sizes (20 mm, 25 mm, 30 mm, and 40 mm). The load–deflection behavior of the control beam was investigated for these mesh sizes, with the smallest mesh size selected to be greater than the 25 mm coarse aggregate size, as shown in Figure 18. The results revealed that mesh sizes of 20 mm, 25 mm, and 30 mm produce similar predictions of the linear and postpeak behavior of the experimental load–deflection curves.

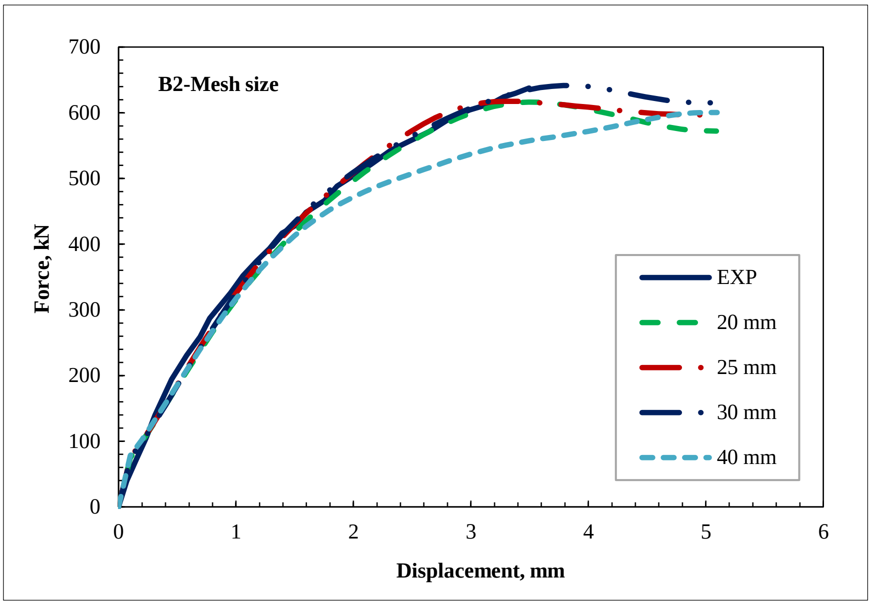

Figure 18. Influences of the mesh size

The 20 mm mesh size provided the most accurate prediction of the ultimate load and postpeak softening response, as it captured localized stress and strain concentrations at the crack and interaction surfaces between the concrete and rebars. Similarly, the 25 mm and 30 mm meshes predicted the experimental ultimate load with 3% and 4% error, respectively, indicating that increasing the mesh size can still produce reliable results. However, the 40 mm mesh size failed to predict the ultimate load and residual softening behavior. This variation is attributed to the inability of larger mesh sizes to detect local stress gradients effectively and their redistribution.

As the mesh size was refined, the number of elements and degrees of freedom at each node exponentially increased, as shown in Table 5. Consequently, adopting a 20 mm mesh size led to a computational time approximately twice that of the 25 mm mesh, six times that of the 30 mesh, and twelve times that of the 40 mm mesh. The extra computational cost corresponding to the 20 mm mesh was significant regardless of the enhanced accuracy. Notably, the 20 mm mesh predicted the ultimate load with only a 1% error compared with the 25 mm mesh, showing that further refinement resulted in negligible accuracy enhancement while increasing the computational cost.

Table 5. Summary of the mesh size, computational time, and number of elements

Mesh size (mm)	Computational time (minute)	Numbers of the concrete element
20	72	18,000
25	36	9,216
30	12	5,880
40	6	2,250

The damage parameters consider the reduction in stiffness after the concrete reaches its crushing and cracking strength, represented by tensile damage (d_t) and compression damage (d_c). Figure 19 illustrates the impact of the damage parameter on the load–deflection behavior. The initial values of the damage parameters (d_t and d_c) were selected on the bases of previous studies, and were used as reference points for a sensitivity analysis. This analysis evaluated their impact on the FEA model's stiffness, ultimate load, and postpeak behavior. When the damage parameters are neglected (d_t=d_c=0), the model underestimates the ultimate load capacity. This can be attributed to the model considering the permanent deformation of the concrete after yielding (plastic strain) while ignoring the strain caused by damage stiffness degradation. Consequently, the residual softening behavior is not captured, as the model ignores the stiffness degradation of the concrete in the post yield surface. Activating only the tensile damage parameter ($d_t \neq 0$, $d_c=0$) leads the model to over predict the experimental ultimate load. This can be attributed to the tension stiffening effect, wherein the model assumes that the reinforcement primarily carries the stress after the concrete cracks. As a result, the crack growth is reduced, which results in a higher ultimate load prediction than the experimental result. Conversely, when only compression damage is considered ($d_c \neq 0$, $d_t=0$), the model underestimates the ultimate load. This underestimation arises from the formation and spread of cracks resulting from neglected tensile stress. As a result, the postpeak softening curve also gradually decreased, which indicates that the model accounts for only compressive degradation. When both compressive damage and tensile damage ($d_t \neq 0$, $d_c \neq 0$) are incorporated, the model appropriately predicts the initial stiffness, ultimate load, and residual softening behavior. This can be attributed to its ability to capture the combined effect of tensile crack development and compressive crushing, representing the nonlinearity of concrete. Overall, tensile and compression damage significantly influence the model and are essential for predicting the strength and stiffness degradation and understanding the failure mechanism.

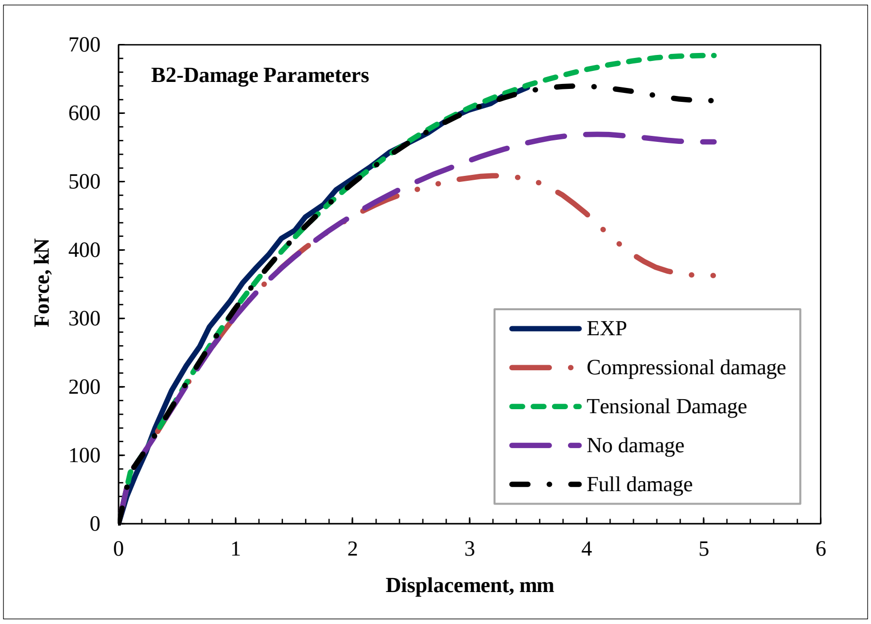

Figure 19. Influence of the damage parameter

5. Numerical Analysis Results

Three shallow reinforced concrete beams reported by Soliman et al. [2, 7] are used for validation. Table 6 compares the load-to-midspan deflection between the FEA and experimental results. The maximum errors between the FEA and the experimental ultimate load and the corresponding deflection are 1.69% and 10.7%, respectively, indicating a strong agreement. In 5.1, 5.2, and 5.3, further analysis of the FE results was presented to investigate the load–deflection behavior, failure pattern, and failure mechanism of wide beams.

Table 6. Comparison of the experimental and FEA results

Beam	$F_{u, EXP}$ (kN)	$F_{u, FEA}$ (kN)	F_{error} (%)	$\Delta_{u, EXP}$ (mm)	$\Delta_{u, FEA}$ (mm)	Δ_{error} (%)
B1	660	649	1.69	4.5	5.04	10.7
B2	640	637	0.47	3.5	3.69	5.1
B3	903	890	1.46	5.7	6.07	6.1

Note: $F_{u, EXP}$, $F_{u, FEA}$, F_{error}, $\Delta_{u, EXP}$, $\Delta_{u, FEA}$, Δ_{error} represents the experimental ultimate load, FE ultimate load, load variation $((F_{u, EXP} - F_{u, FEA})/ F_{u, FEA})$, experimental deflection at the corresponding load, FE deflection at the corresponding load, deflection variation $((\Delta_{u, EXP} - \Delta_{u, FEA})/\Delta_{u, FEA})$, respectively.

5.1. Load-Deflection Curves of the Samples

The load–to–midspan deflection curves of the experimental test and the finite element analysis results were compared for B1, B2, and B3, as shown in Figures 20 to 22. All the results exhibited similar behavior in the elastic stage, whereas the FEA result was stiffer than the experimental result. The reason for the high stiffness was that FEA uses linear properties in the elastic stage; however, actual concrete has some nonlinearity in the elastic stage due to microcracks.

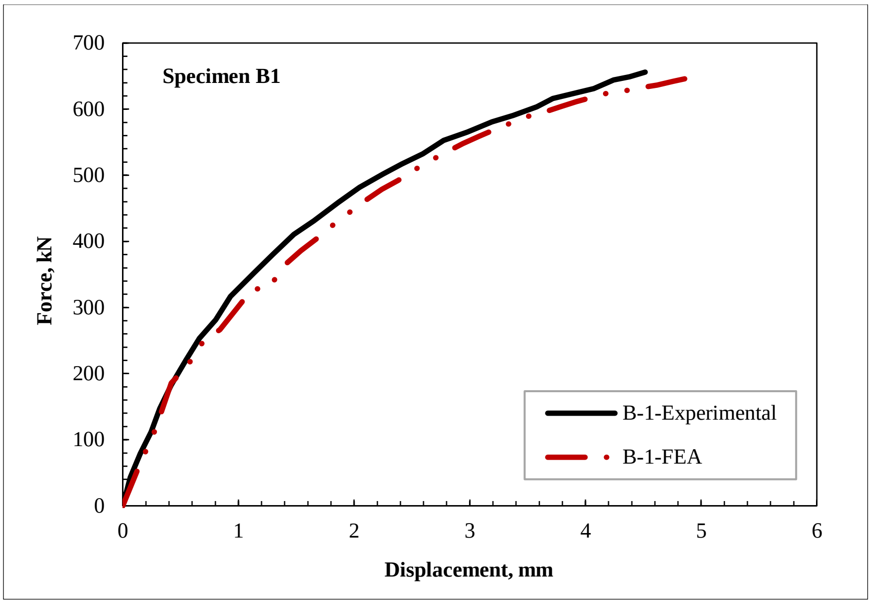

Figure 20. Load–deflection curve for B1

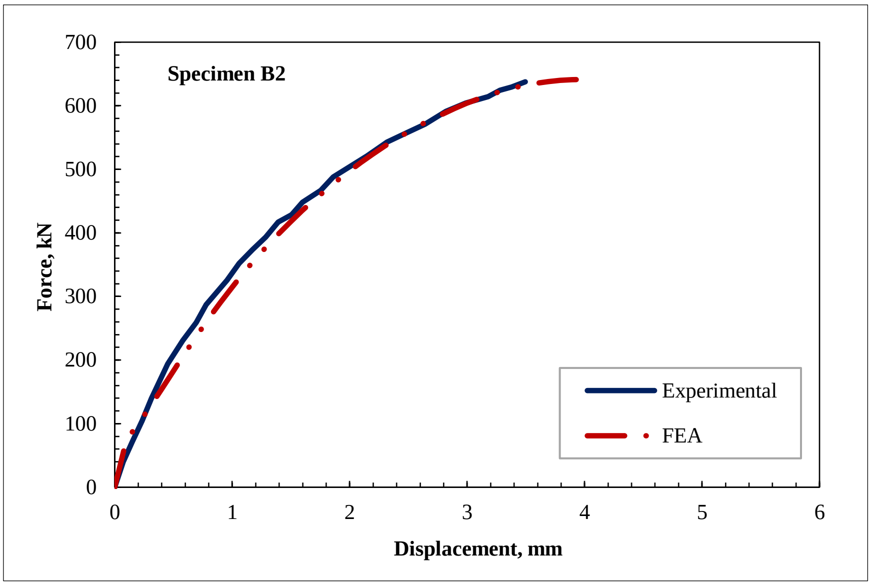

Figure 21. Load–deflection curve for B2

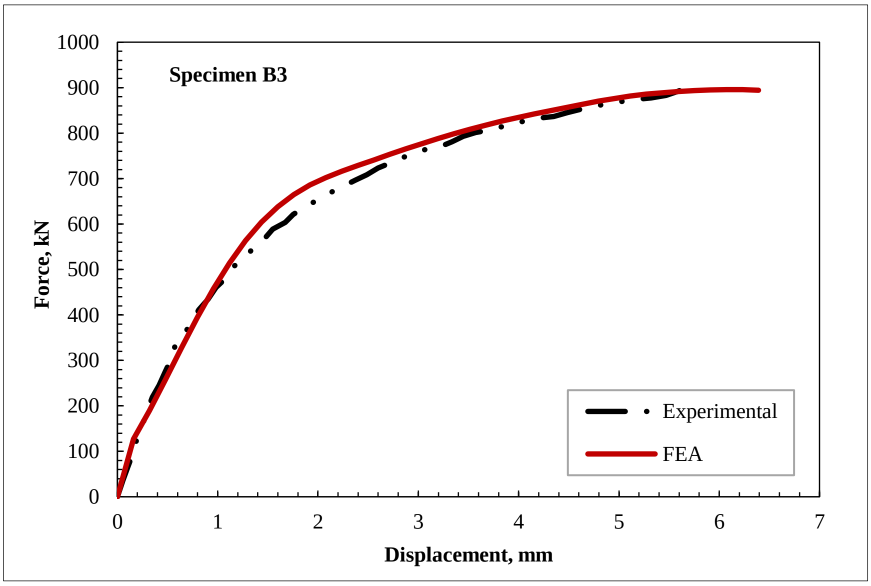

Figure 22. Load–deflection curve for B3

After the elastic stage, the FEA curve shows a gradual loss of stiffness relative to the experimental result. This is attributed to inelastic strain development modelled in Abaqus, which is governed by concrete damage parameters. This inelastic strain is expressed in terms of tensile damage, which is responsible for cracking, and compression damage, which accounts for crushing. This scenario expresses the transition of the elastic behavior of the beam to the inelastic behavior with some reduced stiffness compared with the experimental observations. When the load reaches the ultimate value, the stiffness slightly decreases because the inelastic strain approaches the maximum cracking and crushing strain, resulting in ductile shear failure. Overall, the load–to–midspan deflection of the FEA accurately predicts the experimental results.

5.2. Failure Mechanism of the Samples

A comparison of Figures 23 to 25 reveals that the experimental failure mechanism for wide beams B1, B2, and B3 agrees well with the FEA results. During the initial stages of loading, flexural cracks were observed at the mid-bottom side of the simulated beam, and as loading increased, these cracks propagated and increased in number. This is due to the concrete damage plasticity model, which accounts for the increasing loads leading to an increasing plastic strain, along with damage parameters approaching the critical value of 1 (full crack or crush). Additionally, diagonal cracks were observed near the support, converging toward the location of the applied load. Notably, Figures 24 and 25 exhibit enhanced crack development control attributed to the high density of stirrups, which provide greater confinement and resistance to shear stress. Conversely, Figure 23 shows more crack development due to the light density of the stirrups, which reduces the beam shear capacity. Figure 26 shows the plastic strain distribution in the reinforcement. The results revealed that the stirrups yielded before the longitudinal bar, indicating that the beam exhibited shear failure primarily, which was consistent with the experimental findings.

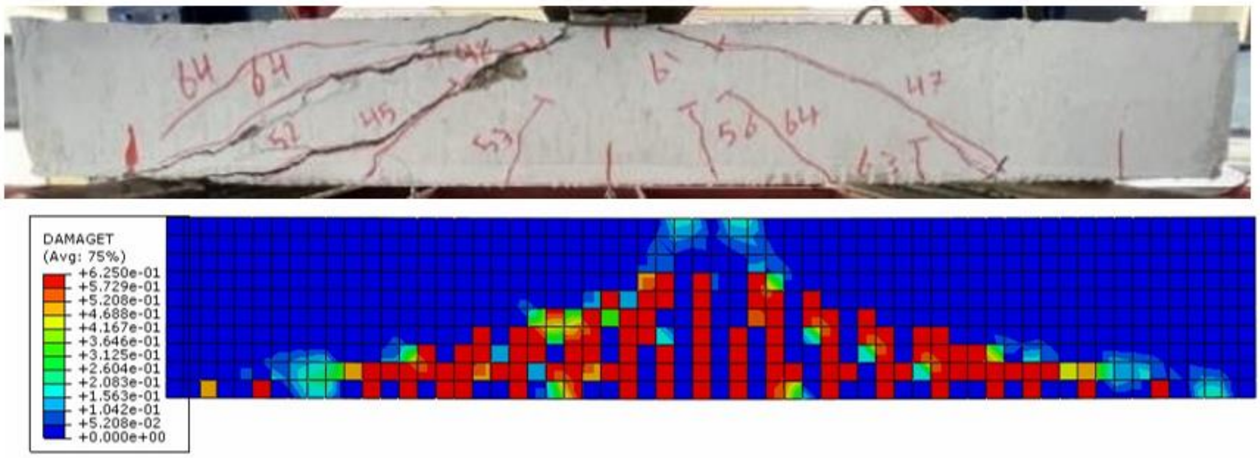

Figure 23. Experimental crack pattern and FEA damage pattern of B1

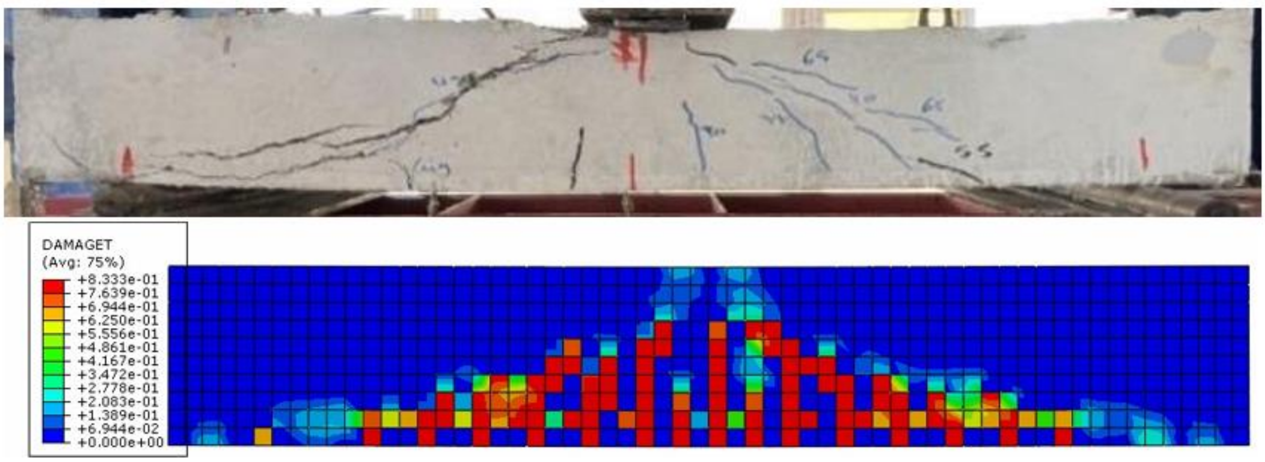

Figure 24. Experimental crack pattern and FEA damage pattern of B2

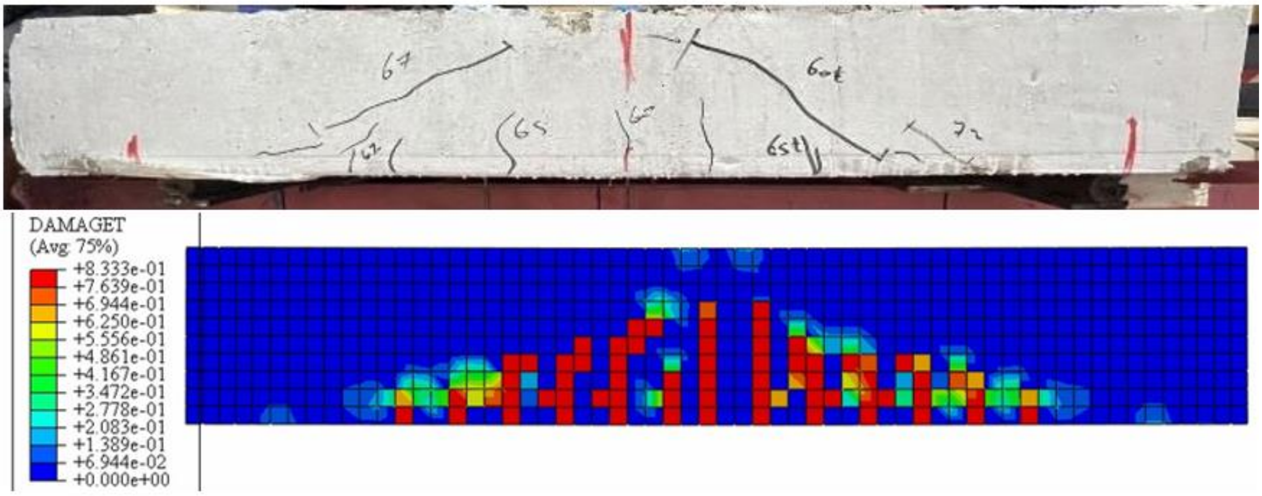

Figure 25. Experimental crack pattern and FEA damage pattern of B3

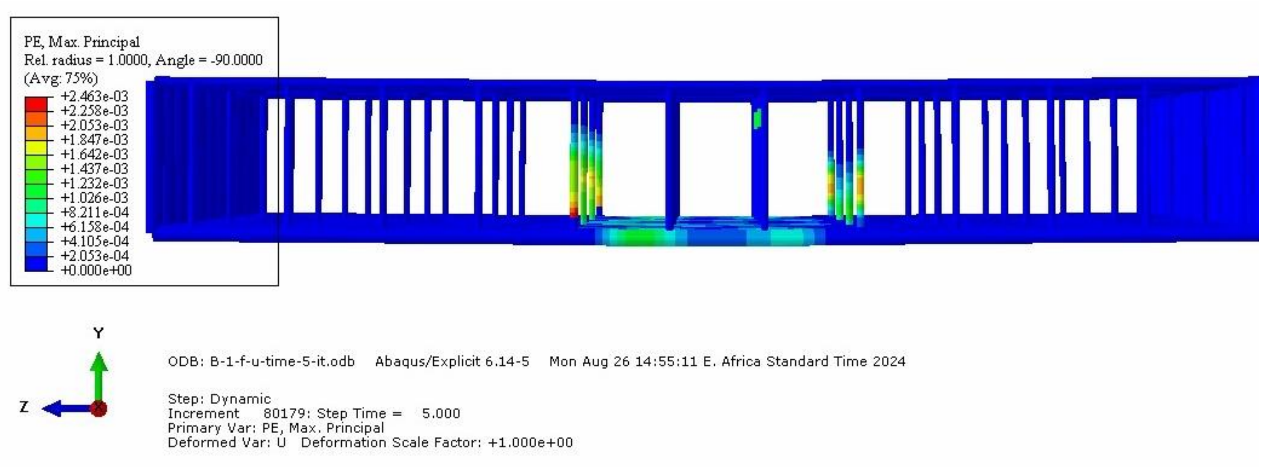

Figure 26. Plastic strain distribution of the reinforcement

5.3. Effects of the Stirrup Spacing, Beam Width, and Longitudinal to Shear Reinforcement Ratio

The influences of the stirrup spacing, width of the shallow beam, and ratio of longitudinal to shear reinforcement are illustrated in Figure 27. All the beams (B1, B2, and B3) share a uniform longitudinal reinforcement ratio of 3.73% (ρl=As/(bd)). However, their transverse reinforcement ratios differ: B1 and B3 have a ratio of 0.33%, whereas B2 has a ratio of 0.42%. On the basis of the FEA and the experimental investigation, the following observations were made:

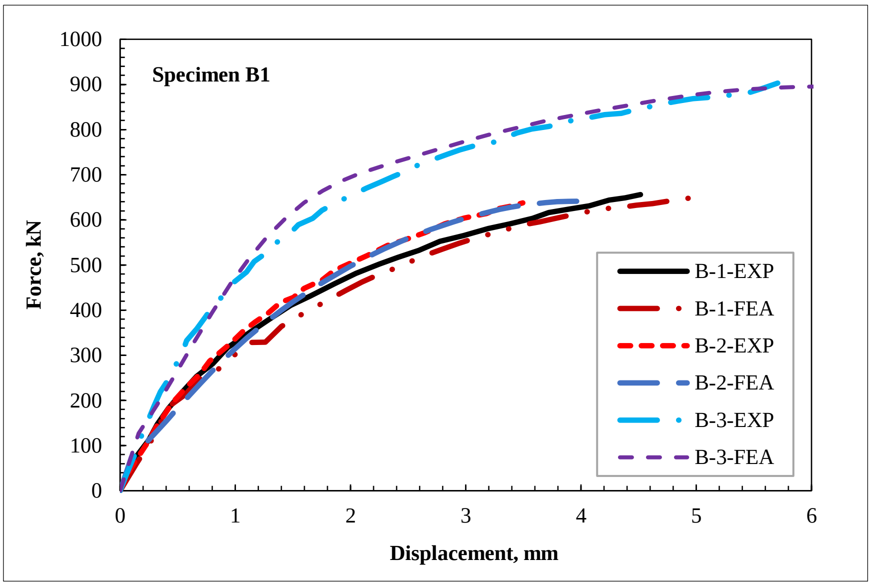

Figure 27. Load–deflection curves for all experimental and FEA shallow beams

Since all wide RC beams use the same concrete (31 MPa) and reinforcement (233 MPa and ρl=3.73%), they exhibit similar stiffnesses in the elastic region (approximately 90 kN). The FEA result captures this initial stiffness well.

A comparison of beams B1 and B2 shows the impact of changing the transverse reinforcement ratios. While their sectional and material properties are the same, B1 has a transverse reinforcement ratio of 0.33% (4 legs Ø 8 mm with 100 mm spacing), whereas B2 has a higher ratio of 0.42% (4 legs Ø 6 mm with 45 mm spacing). The results revealed that increasing the stirrup ratio increased the stiffness and crack development (Figures 23 and 24) and improved ductility but slightly reduced the shear strength. This improvement was attributed to the confinement effect of the stirrups, which strengthened the concrete compression strength.

Examining wide RC beams B1 and B3 focuses on the influence of beam width and stirrup arrangement. Regardless of the exact longitudinal and transverse ratios (3.73% and 0.33%, respectively), B3 is characterized by an increased width size (900 mm) and a modified stirrup configuration (5 legs Ø 8 mm with 100 mm spacing). This change resulted in superior strength, stiffness, limited cracks (Figures 23 and 25), and postpeak ductility for B3 compared with those of B1 and B2. The larger cross-sectional area and closed-leg stirrup arrangement in B3 enhanced the concrete confinement by improving the shear strength performance. Furthermore, a wider beam can distribute stress efficiently over a larger area, which results in a higher shear strength.

The longitudinal to transverse (LR/TR) ratio further emphasizes the relationship between the rebar distribution and shear capacity. B1, B2, and B3 had LR/TR ratios of 11.3%, 8.88%, and 11.3%, respectively. The results revealed that a higher LR/TR ratio increases the shear strength, as shown in B1 and B3. This improvement was due to the high amount of longitudinal reinforcement confining the concrete, which enhances the compressive strength and delay of cracking (Figures 24 and 25).

5.4. Code Comparison and FEA Predictions

A comparison was made between the experimental results of the shear strength of wide RC beams with the FEA, Eurocode, and ACI results, as shown in Table 8. The ACI calculates the shear strength of RC beams by considering the combined strength of the concrete and stirrups via the following Equation:

$$VRD \ = \frac{fcm^{0.5} * bw * d}{6} + \left(\frac{Asw}{s}\right) * d * fywd \tag{10}$$

where b_w is the beam width, d is the effective depth, A_{sw} is the stirrup area, and f_{ywd} is the stirrup design yield strength.

Eurocode assumes that the stirrups resist all the shear stress and uses the variable strut inclination method to compute the shear capacity, as shown in Equation 9.

$$VRD = \ Asw * Z * fywd * (Cot\theta + Cot\alpha) * \frac{Sin\alpha}{s} and\ Z = 0.9d \tag{11}$$

where θ is the inclination angle, which varies from 21.8^0 - 45^0, α is the stirrup angle, Z is the lever arm, and S is the stirrup spacing.

The Fib Modal Code III provides an equation that predicts the shear capacity of RC beams on the basis of modified compression–filling theory, which considers the strength between cracks or tension stiffening via the following Equations.

$$VRD = \frac{Asw}{S} * Z * fywd * \cot\theta + Kv * Z * \sqrt{fcd} * bw \tag{12}$$

$$Kv = \frac{0.4}{1+1500\varepsilon x}\left(1 - \frac{VED}{VRD,max(\theta)}\right) \tag{13}$$

$$VRD,max(\theta) = 0.9 * Kc * fcd * bw * d * \left(\frac{\cot\theta + \cot\alpha}{1+\cot^2\theta}\right) \tag{14}$$

$$\varepsilon x = \frac{1}{2*Es*Asl} * \left(\frac{MED}{Z} + \frac{VED*\cot\theta}{2}\right) \tag{15}$$

where K_v is the contribution of the aggregate to the effective shear area, ε_x is the longitudinal strain at the middle depth of the effective shear area, K_c is the reduction factor that accounts for the concrete business and web strain rate, M_{ED} is the bending moment, and V_{ED} is the shear force. A_{sl} is an area of longitudinal reinforcement.

Using a truss model, De Domenico & Ricciardi [26] improved the Eurocode shear strength prediction equation of RC beams with transverse reinforcement via the following equations.

$$V_{RD} = 3.75 * \frac{Asw}{b * d} * fywd * (bw * z) \tag{16}$$

where ρ_w is the stirrup ratio.

Ebid & Deifalla [27] proposed a machine learning-based equation to predict the shear strength of RC beams with stirrups via genetic programming (GP) techniques.

$$V_{RD} = \frac{1.25\times\ln\left|1.3+0.7\rho_S\times f_{ywd}+0.2\rho_L\right|}{\ln\left|45\times\frac{a}{d}\times\frac{E_{cm}}{E_S}\right|}\times b\times d\times\sqrt{f_{cm}} \tag{17}$$

where ρ_S is the stirrup ratio, ρ_L is the longitudinal reinforcement ratio, a is the shear span length of the beam, and Es is the reinforcement elastic modulus.

Table 7. Summary of experimental, FEA, Eurocode, ACI, modal code, Domenico shear prediction, and GP methods

Beam	$V_{RD, Exp}$	VRD, Exp / VRD, FEA	VRD, Exp / VRD, ACI	VRD, Exp / VRD, EC2	VRD, Exp / VRD, MC	VRD, Exp / VRD, Domenico	VRD, Exp / VRD, GP
B1	330	1.017	2.08	4.6	3.0	2.48	1.44
B2	320	1.005	2.43	3.4	2.13	4.35	1.4
B3	452	1.02	1.9	6.05	2.23	2.26	1.29

The FEA, which uses the CDP model in Abaqus, achieved high accuracy in predicting shear strength, with an experimental-to-predicted ratio of 1.017 for B1, as shown in Table 8. This accuracy originates from the CDP model's ability to capture the nonlinear behavior of concrete, including tensile and compressive plasticity, residual strength between cracks (tension stiffening), and damage parameters. In comparison, the ACI method overestimates the shear strength at a ratio of 2.08, indicating a lower accuracy of the experimental results. The ACI approach considers the contributions of concrete and stirrups; however, it neglects essential factors such as crack development, tension stiffening, and nonlinear reinforcement behavior, leading to reduced accuracy.

Eurocode, with a ratio of 4.6, produces highly conservative results because the stirrups resist all the shear stress effectively, ignoring the contribution of the concrete. The Fib Modal Code gives moderately conservative predictions with a ratio of 3, gaining an advantage for introducing tension stiffening. However, its partial consideration of non-linear concrete behavior makes it less accurate than FEA. De Domenico & Ricciardi [26] incorporated the truss model in Eurocode, accounting for stress redistribution at the crack regions, whose prediction ratio is 2.48, offering better agreement with the experimental results than the Eurocode and Fib Modal Code.

For B2, the FEA achieves an experiment-to-predict ratio of 1.005, precisely capturing the reduced area of the stirrups. Conversely, the ACI, Eurocode, Fib Modal Code, and De Domenico & Ricciardi [26] models fail to capture the effects of the decreasing stirrup area, resulting in prediction ratios of 2.43, 2.13, 3.1, and 4.35, respectively. For B3, the FEA again demonstrates its accuracy, with a ratio of 1.02, accurately predicting the influence of increased beam width and stirrup area. The ACI gives the next best prediction with a ratio of 1.9, followed by the Fib Modal Code (2.23) and De Domenico & Ricciardi [26] (2.26). However, Eurocode significantly underestimates the shear capacity, with a ratio of 6.05, reflecting its excessively conservative prediction.

In summary, FEA provides greater accuracy in predicting the shear strength of a shallow RC beam than the traditional design codes developed for conventional RC beams. However, genetic programming (GP) becomes a strong option, performing accurate predictions for beams B1, B2, and B3 with experimental-to-predicted ratios of 1.44, 1.4, and 1.29, respectively. This comparison among FEA, codes, and genetic programming emphasizes the importance of choosing design codes for shallow RC beams to satisfy safety requirements and optimization.

6. Conclusions

A numerical investigation of the shear behavior of a wide RC beam was performed via Abaqus software. Three samples with different stirrup spacing and widths of the beam were extracted from the experimental test to simulate their load–deflection curve and failure mechanisms. Concrete damage plasticity was used to model the behavior of the concrete, and the CDP parameter values were calibrated to improve the accuracy of the FE model prediction. The following conclusions were drawn from the FE results.

- The FEA captured the ultimate load and corresponding deflection with maximum variations of 1.69% and 10.7%, respectively, which agreed with the test results. Furthermore, the cracking pattern and failure mechanism of the concrete were accurately captured, and the maximum plastic strain of the reinforcement also aligned with the test findings.
- Selecting the dilation angle, Kc values, and damage parameters from the CDP parameters significantly influences the model behavior.
- The dilation angle values (ranging from 30° to 46°) significantly influence the load-deflection behavior after the elastic limit, and the appropriate dilation angle for a shallow RC beam is 32°.

- Neglecting tension damage resulted in an underestimation of the shear strength, whereas neglecting compression damage resulted in an overestimation of the shear strength. Assigning proper damage parameters results in a better estimation of the FE model.
- In quasi-static analysis, viscosity does not affect the accuracy of the FE result; however, the loading time significantly impacts the model, and increasing the loading time increases the computational time and accuracy.
- Increasing the stirrup ratio increases the stiffness and ductility without significantly improving the shear strength. On the other hand, increasing the width and longitudinal-to-transverse reinforcement ratio enhances the strength and ductility**.**
- The FEA prediction sets the highest standard for accurate shear strength predictions, whereas GP is the second-best machine learning method. Although the truss model and Fib Modal Code provide enhancements based on the basis of traditional codes, they are far from accurate in terms of FEA and GP.

7. Declarations

7.1. Author Contributions

Conceptualization, H.D. and M.B.; methodology, H.D. and M.B.; software, H.D. and M.B.; validation, H.D., M.B., and M.R.; formal analysis, H.D. and M.B.; investigation, H.D. and M.B.; resources, H.D., M.B., and M.R.; data curation, H.D. and M.B.; writing—original draft preparation, H.D. and M.B.; writing—review and editing, H.D., M.B., and M.R.; visualization, H.D., M.B., and M.R.; supervision, M.B.; project administration, H.D.; funding acquisition, H.D. All authors have read and agreed to the published version of the manuscript.

7.2. Data Availability Statement

The data presented in this study are available in the article.

7.3. Funding

The authors received no financial support for the research, authorship, and/or publication of this article.

7.4. Conflicts of Interest

The authors declare no conflict of interest.

8. References

[1] Elansary, A. A., Elnazlawy, Y. Y., & Abdalla, H. A. (2022). Shear behaviour of concrete wide beams with spiral lateral reinforcement. Australian Journal of Civil Engineering, 20(1), 174–194. doi:10.1080/14488353.2021.1942405.

[2] Soliman, A. A., Mansour, D. M., Khalil, A. H., & Ebid, A. (2023). The Impact of Aspect Ratio, Characteristic Strength and Compression Rebars on the Shear Capacity of Shallow RC Beams. Civil Engineering Journal (Iran), 9(9), 2259–2271. doi:10.28991/CEJ-2023-09-09-012.

[3] Elsayed, M., Badawy, S., Tayeh, B. A., Elymany, M., Salem, M., & ElGawady, M. (2022). Shear behaviour of ultra-high performance concrete beams with openings. Structures, 43, 546-558. doi:10.1016/j.istruc.2022.06.071.

[4] Alluqmani, A. E. (2020). Effect of the transversal-spacing of stirrup-legs on the behavior and strength of shallow concealed RC beams. Journal of Engineering, Design and Technology, 19(4), 932–942. doi:10.1108/JEDT-06-2020-0224.

[5] Hafezolghorani, M., Hejazi, F., Vaghei, R., Jaafar, M. S. Bin, & Karimzade, K. (2017). Simplified damage plasticity model for concrete. Structural Engineering International, 27(1), 68–78. doi:10.2749/101686616X1081.

[6] Mahmoud, S. M., Mabrouk, R. T. S., & Kassem, M. E. (2021). Behavior of RC wide beams under eccentric loading. Civil Engineering Journal (Iran), 7(11), 1880–1897. doi:10.28991/cej-2021-03091766.

[7] Soliman, A. A., Mansour, D. M., Khalil, A. H., & Ebid, A. (2023). The Impact of Shear Reinforcement Amount and Arrangement on the Shear Capacity of Shallow RC Beams: An Experimental Study. Civil Engineering Journal (Iran), 9(12), 3147–3160. doi:10.28991/CEJ-2023-09-12-013.

[8] Said, M., & Elrakib, T. M. (2013). Enhancement of shear strength and ductility for reinforced concrete wide beams due to web reinforcement. HBRC Journal, 9(3), 235–242. doi:10.1016/j.hbrcj.2013.05.011.

[9] Luk, S. H., & Kuang, J. S. (2017). Seismic performance and force transfer of wide beam-column joints in concrete buildings. Proceedings of the Institution of Civil Engineers: Engineering and Computational Mechanics, 170(2), 71–88. doi:10.1680/jencm.15.00024.

[10] Luu, X. B., Kim, S. K., & Kim, W. (2023). Investigation of Load–Displacement Characteristics and Crack Behavior of RC Beam Based on Nonlinear Finite Element Analysis Using Concrete Damage Plasticity. Applied Sciences (Switzerland), 13(21), 11798. doi:10.3390/app132111798.

[11] Rai, P. (2021). Non-Linear Finite Element Analysis of RC Deep Beam Using CDP Model. Advances in Technology Innovation, 6(1), 01–10. doi:10.46604/aiti.2021.5407.

[12] Al-Sebai, H., Al-Sadoon, Z. A., Altoubat, S., & Maalej, M. (2024). Constitutive Relations for Modelling Macro Synthetic Fiber Reinforced Concrete. Civil Engineering Journal, 10(6), 1806-1827. doi:10.28991/CEJ-2024-010-06-06.

[13] Behnam, H., Kuang, J. S., & Samali, B. (2018). Parametric finite element analysis of RC wide beam-column connections. Computers & Structures, 205, 28–44. doi:10.1016/j.compstruc.2018.04.004.

[14] Raza, A., Khan, Q. U. Z., & Ahmad, A. (2019). Numerical investigation of load-carrying capacity of GFRP-reinforced rectangular concrete members using CDP model in Abaqus. Advances in Civil Engineering, 2019(1), 1745341. doi:10.1155/2019/1745341.

[15] Genikomsou, A. S., & Polak, M. A. (2015). Finite element analysis of punching shear of concrete slabs using damaged plasticity model in ABAQUS. Engineering Structures, 98, 38–48. doi:10.1016/j.engstruct.2015.04.016.

[16] Silva, L. M. e, Christoforo, A. L., & Carvalho, R. C. (2021). Calibration of Concrete Damaged Plasticity Model parameters for shear walls. Matéria (Rio de Janeiro), 26(1). doi:10.1590/s1517-707620210001.1244.

[17] Szczecina, M., & Winnicki, A. (2017). Relaxation Time in CDP Model Used for Analyses of RC Structures. Procedia Engineering, 193, 369–376. doi:10.1016/j.proeng.2017.06.226.

[18] Khalil, A. E. H., Etman, E., Atta, A., Baraghith, A., & Behiry, R. (2019). The Effective Width in Shear Design of Wide-shallow Beams: A Comparative Study. KSCE Journal of Civil Engineering, 23(4), 1670–1681. doi:10.1007/s12205-019-0830-7.

[19] EN 1998-1. (2004) Euro Code 8-Design of Structures for Earthquake Resistance-Part 1: General Rules, Seismic Actions and Rules for Buildings. Brussels, Belgium.

[20] Moubarak, A. M. R., Elwardany, H., Abu El-hassan, K., & El-Din Taher, S. (2022). Shear strengthening of wide-shallow beams by inserted fasteners. Engineering Structures, 268, 114554. doi:10.1016/j.engstruct.2022.114554.

[21] Akinpelu, M. A., Gabriel, D. S., Salman, A. M., & Raheem, I. A. (2023). Numerical study on the effect of different column shapes on punching shear behavior of flat slabs. Results in Engineering, 19, 101345. doi:10.1016/j.rineng.2023.101345.

[22] Soliman, A. A., Mansour, D. M., Khalil, A. H., & Ebid, A. (2024). Predictive modeling of wide-shallow RC beams shear strength considering stirrups effect using (FEM-ML) approach. Scientific Reports, 14(1), 12523. doi:10.1038/s41598-024-62532-y.

[23] ABAQUS (2024). Abaqus Finite Element Analysis | SIMULIA. Dassault Systèmes و Vélizy-Villacoublay, France.

[24] Allam, S. M., Shoukry, M. S., Rashad, G. E., & Hassan, A. S. (2013). Evaluation of tension stiffening effect on the crack width calculation of flexural RC members. Alexandria Engineering Journal, 52(2), 163–173. doi:10.1016/j.aej.2012.12.005.

[25] Wosatko, A., Pamin, J., & Polak, M. A. (2015). Application of damage–plasticity models in finite element analysis of punching shear. Computers & Structures, 151, 73-85. doi:10.1016/j.compstruc.2015.01.008.

[26] De Domenico, D., & Ricciardi, G. (2019). Shear strength of RC beams with stirrups using an improved Eurocode 2 truss model with two variable-inclination compression struts. Engineering Structures, 198, 109359. doi:10.1016/j.engstruct.2019.109359.

[27] Ebid, A. M., & Deifalla, A. (2021). Prediction of shear strength of FRP reinforced beams with and without stirrups using (GP) technique. Ain Shams Engineering Journal, 12(3), 2493-2510. doi:10.1016/j.asej.2021.02.006.